JOURNAL OF GEOPHYSICAL RESEARCH, VOL. 114, E04004, doi:10.1029/2008JE003300, 2009

Regionally compartmented groundwater flow on Mars

Keith P. Harrison[1] and Robert E. Grimm[1]

Received 13 November 2008; revised 23 January 2009; accepted 10 February 2009; published 1 April 2009.

[1] Groundwater flow on Mars likely contributed to the formation of several types of morphologic and mineralogic features, including chaotic terrains, valley networks, Meridiani Planum geologic units and, potentially, sulfate and phyllosilicate deposits. A central issue for these features is the spatial scale of groundwater flow required for their formation. For groundwater simulation purposes, a global Martian aquifer has frequently been assumed, but the validity of this assumption has not been tested. Chaotic terrains, thought to have formed owing to the disruption of a cryosphere under high aquifer pore pressures, provide the basis for such a test. Specifically, we use groundwater models to predict regions of cryosphere disruption due to recharge-driven pore pressure increases, and we compare these regions to observed Martian chaotic terrains. Our results suggest that a globally connected aquifer cannot give rise to cryosphere disruption at the two locations where large chaotic terrains are observed (the circum-Chryse region and the eastern Hellas Planitia). Conversely, modeled cryosphere disruption occurs in locations such as Amazonis Planitia and west Hellas Planitia where no supporting evidence is present, suggesting again that groundwater flow was likely regionally compartmented. Furthermore, the consistent occurrence of modeled breakouts in the Valles Marineris canyon system suggests that large-scale fractures there likely discharged most of the groundwater required for circum-Chryse outflow channel formation, with only minor contributions from chaotic terrains. The fractures are close to a likely source of recharge over Tharsis, and their low elevations lead to high pore pressures even if groundwater flow is regionally compartmented.

Citation: Harrison, K. P., and R. E. Grimm (2009), Regionally compartmented groundwater flow on Mars, *J. Geophys. Res.*, *114*, E04004, doi:10.1029/2008JE003300.

1. Introduction

[2] Groundwater is thought to have influenced erosion or weathering processes involved in the formation of large Martian fluvial features, including outflow channels [*Carr*, 1979; *Baker*, 1982] and valley networks [*Craddock and Howard*, 2002; *Luo and Howard*, 2008]. Groundwater may also have contributed to the formation of sulfates and phyllosilicates detected at several locations on Mars [*Gendrin et al.*, 2005; *Poulet et al.*, 2005], and a variety of bedrock outcrop features observed by the Mars Exploration Rover Opportunity at Meridiani Planum [*Grotzinger et al.*, 2005]. The spatial distribution of these phenomena suggests that groundwater flow might once have been widespread on Mars. Indeed, Martian groundwater simulations to date have assumed laterally uniform permeabilities capable of supporting global-scale flows [e.g., *Harrison and Grimm*, 2004; *Andrews-Hanna and Phillips*, 2007]. *Clifford* [1993] argued that in terrestrial crust the pervasive presence of fracturing prevents any large-scale geologic formation from being considered impermeable, implying (for both the earth and Mars) that lateral hydraulic connectivity is essentially unlimited. Global-scale groundwater flows are not, however, observed terrestrially because high precipitation rates shape the water table to a subdued replica of the topography, limiting hydraulic gradients to small spatial scales [*Tóth*, 1963]. Arid climates allow at most regional-scale groundwater flows (e.g., the Great Basin province, North America; the Great Artesian Basin, Australia; the Nubian Aquifer System in the eastern Sahara) [*Clifford*, 1993]. If the terrestrial and Martian crusts are hydrologically similar, the globally arid nature of Mars may have allowed truly global flows to have occurred. However, the wide distribution of groundwater-related features on Mars does not explicitly require global-scale flow: groundwater may have circulated in isolated local- to regional-scale aquifers. Indeed, there is no direct observational evidence for global-scale groundwater flow on Mars. It is, however, possible to test the viability of global-scale flow, and we suggest that chaotic terrains provide the basis for such a test. Chaotic terrains are large (tens of kilometers) randomly arranged blocks resulting from the collapse of an ice-filled permafrost layer (cryosphere) during the Hesperian and early Amazonian epochs. The close association of chaotic terrains with the head regions of large flood channels suggests that collapse was initiated by high aquifer pore pressures exerted on the cryosphere from below [*Carr*, 1979, 1996]. The failure of the cryosphere allowed pore pressures to be released through the discharge of large volumes of groundwater to the surface. Chaotic terrains thus serve as markers for high pore pressures in the Martian aquifer. A groundwater simu-

[1]Southwest Research Institute, Boulder, Colorado, USA.

0148-0227/09/2008JE003300$09.00

Table 1. Parameters Used in the Groundwater Model Governing Equations and in the Calculation of Cryosphere Thickness

Parameter Description	Symbol Used in Text	Value
Aquifer		
Pore fluid density	ρ	10^3 kg/m^3
Pore fluid dynamic viscosity	μ	10^{-3} Pa s
Gravitational acceleration	g	3.7 m/s^2
Depth-averaged permeability (nominal model)	k	1.9×10^{-16} to 1.7×10^{-14} m^2
Depth-averaged porosity (nominal model)	n	0.0033 to 0.0058
Depth-averaged rock matrix compressibility	α	5×10^{-10} Pa^{-1}
Pore fluid compressibility	β	4.8×10^{-10} Pa^{-1}
Cryosphere		
Pore ice density	ρ_{ice}	10^3 kg/m^3
Rock matrix density	ρ_{rock}	2500 kg/m^3
Surface temperature at poles[a]		177 K
Surface temperature at equator[a]		209 K
Geothermal gradient[b]		30 mW m^{-2}
Thermal conductivity of cryosphere		2 W/(m K)

[a] *Haberle et al.* [2003].
[b] The approximate mean Hesperian value from *McGovern et al.* [2002].

lation that responds to high pore pressures with a cryosphere disruption mechanism can thus be used to search for global-scale groundwater flow patterns consistent with observed chaotic terrain locations. This approach can also test the assumption made in several existing groundwater models that high pore pressures for cryosphere disruption at a given location are always available as needed [*Carr*, 1979; *Manga*, 2004; *Hanna and Phillips*, 2005; *Andrews-Hanna and Phillips*, 2007; *Harrison and Grimm*, 2008].

[3] In this paper we implement the above approach numerically. Our groundwater model employs aquifer recharge as a means of generating high pore pressures, and includes alternative recharge locations, threshold pressures required for cryosphere disruption, and approaches to topography. A stochastic approach is used to generate a variety of heterogeneous permeability distributions. We proceed with a description of the model, followed by a presentation of our key results and their ramifications.

2. Model

[4] We simulate groundwater flow using the U.S. Geological Survey MODFLOW finite difference code [*McDonald and Harbaugh*, 1988; *Harbaugh et al.*, 2000], the de facto standard in terrestrial groundwater modeling [*Domenico and Schwartz*, 1998]. We have used MODFLOW extensively in previous Martian groundwater studies [*Harrison and Grimm*, 2004, 2008] and we have adapted it to spherical shell geometry for more accurate global modeling. The dependent variable is hydraulic head, which expresses aquifer pore pressure as the equivalent rise height of pore fluid in a thin vertical tube (manometer) imbedded in the aquifer. Further details of the model implementation can be found in Appendix A and Table 1.

2.1. Concept

[5] Conceptually, our model follows the sequence of events depicted in Figure 1. A global aquifer with an initially uniform water table is recharged by meltwater produced at the base of a hypothetical ice sheet. This process has been suggested for both the south polar region of Mars [*Clifford*, 1993] and, at high planetary obliquities, for the Tharsis rise [*Harrison and Grimm*, 2004; *Coleman et al.*, 2007; *Russell and Head*, 2007]. Indeed, recharge appears to be a prerequisite for circum-Chryse outflow channel formation, since the volume of water required for channel erosion greatly exceeds that which can be stored instantaneously in parts of the aquifer accessible to the channels [*Harrison and Grimm*, 2004]. Downward infiltration of meltwater locally raises the water table, producing lateral hydraulic gradients that drive groundwater radially outward to other parts of the aquifer. Pore pressures rise regionally (and eventually globally) and, at some location determined by elevation and proximity to the recharge zone, reach a value high enough to open fractures in the cryosphere through which groundwater can reach the surface (a process henceforth called ''breakout''). The threshold pressure at which breakout occurs depends on the state of the cryosphere. An end-member case is a strong, poorly fractured cryosphere which is disrupted only if underlying aquifer pore pressures are able to exceed the weight of the cryosphere; that is, they must reach superlithostatic values. This is the nominal approach taken here, although we later consider disruption at lower pressures. Surface discharge due to breakout may produce ponding and channel incision (which we do not model here), but it also influences the aquifer by depressing local (and eventually regional) pore pressures, preventing further breakouts close to the original site. Distal breakouts may, however, be possible and their location will be influenced not only by topography and proximity to recharge, but by regional changes in pore pressure induced by preceding breakouts. The location of breakouts, and therefore of chaotic terrains and outflow channels, is thus determined by an interplay between recharge location, topography, and the dynamical history of groundwater flow. Simple analytic approaches to this system are not available, hence the need for a self-consistent numerical model.

2.2. Permeability

[6] Of particular importance to the spatial scale of groundwater flow is the lateral variation of permeability. Terrestrial data [e.g., *Manning and Ingebritsen*, 1999] suggest that Martian crustal permeabilities are likely to vary markedly over a range of spatial scales. More specific inferences concerning Martian permeabilities structure may, perhaps, be possible from remote sensing data. For instance, the possibility

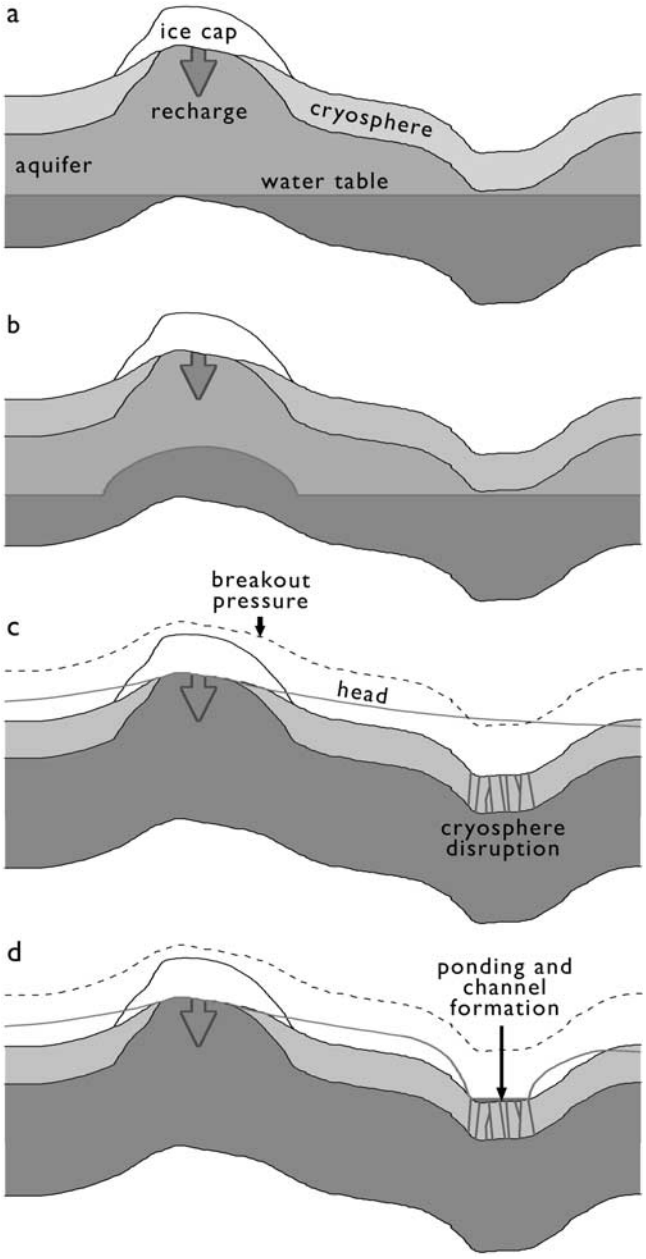

Figure 1. Conceptual representation of our nominal groundwater model. (a) Basal melting at an ice cap recharges an aquifer with an initially uniform water table. (b) A groundwater mound develops beneath the recharge zone, producing flow radially outward to other parts of the aquifer. (c) The aquifer is fully saturated, but increasing pore pressure causes hydraulic head to exceed the lithostatic overburden in places, causing cryosphere disruption. (d) Disruption allows groundwater to escape to the surface (where it ponds and forms channels) and causes local aquifer pore pressures to drop sharply.

of a megaregolith formed by impact gardening suggests higher permeabilities in the top one or two km of crust [*MacKinnon and Tanaka*, 1989] than at greater depths. Observed tectonic structures may indicate preferred groundwater pathways, and geologic units may reflect zones of similar permeability. However, while these inferences are worth pursuing, they have yet to yield firm quantitative constraints (especially on lateral heterogeneity), and no map of permeabilities is thus available. Nonetheless, it is a central goal of this work to explore the spatial scale of Martian groundwater flow, and lateral heterogeneity must therefore be considered. We use a straightforward stochastic approach, drawing values from a normal distribution with a chosen mean and variance (Appendix B). However, because permeability is likely to be correlated over short distances, we need to control the spatial arrangement of permeabilities not represented by one-dimensional statistical measures. We therefore select permeabilities using a variogram with a sill value corresponding to the chosen variance (σ^2), and a range value (R) corresponding to a chosen length scale (Appendix B). Photogeologic units, distinguished by unique surface textures, crater distributions, and topography, may indicate the approximate length scale of shallow permeability variations. At depths pertinent to our groundwater models (tens of km), this relationship is less certain, but the approximate mean diameter of geologic units ($\sim$1000 km or about 15°) nonetheless serves as a rough nominal estimate of length scale.

[7] Because crustal permeabilities may vary spatially over orders of magnitude [*Manning and Ingebritsen*, 1999], we work with its base 10 logarithm. The code we have written to prepare our models takes as a free parameter the surface permeability k_{surf}, from which the depth-averaged value k is computed. We choose -12.65 and 0.5 as the mean and standard deviation of $\log(k_{surf})$, respectively (with k_{surf} expressed in units of m^2; Appendix A). These values, together with the length scale $R = 15°$ and the computations necessary for spherical geometry (Appendix B), allow us to construct a random field of permeability values. However, this single stochastic realization is as probable as any other drawn from the same distribution: Many independent realizations must therefore be considered in order for general conclusions regarding the chosen mean, variance, and length scale to be made. We thus generate 100 independent realizations, each of which is implemented in a separate MODFLOW model.

2.3. Model Parameter Space

[8] In order to consider reasonable alternatives to some of our nominal model assumptions, we extend the explored parameter space. In particular, we implement the following model variations.

2.3.1. South Polar Recharge

[9] We apply recharge to the south polar region [*Harrison and Grimm*, 2004; *Clifford*, 1993] instead of the Tharsis rise, but we leave the recharge area and rate unchanged. Although south polar recharge was likely unable to supply groundwater to the highest circum-Chryse outflow channels [*Carr*, 2002], it may have contributed to lower elevation features.

2.3.2. Predisruption Topography

[10] Because chaotic terrains and outflow channels are traditionally interpreted to be products of cryosphere disruption and groundwater discharge, they are usually assumed to be fully formed only some time after the initial episode(s) of disruption. Our nominal model, however, assumes that significant disruption occurs after the topography of chaos and channels is largely in place. This assumption is made partly because prechannel and prechaos topography is not known, and partly because multiple discharge events are likely at large

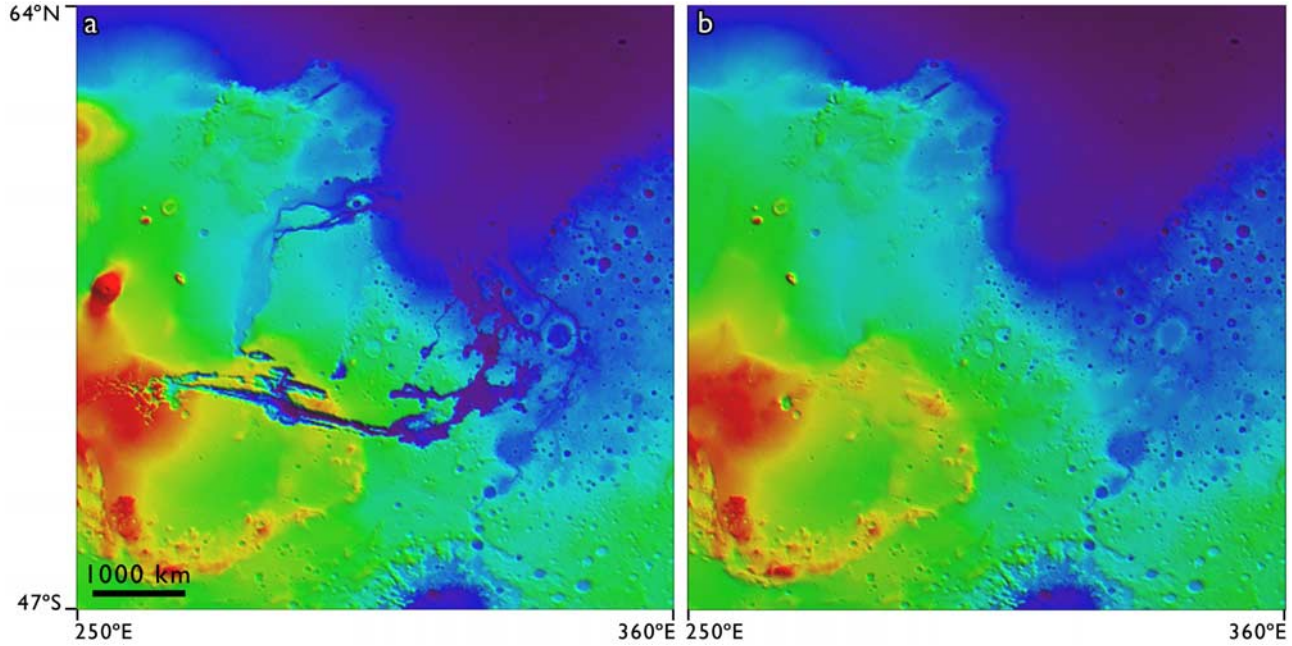

Figure 2. (a) Shaded Mars Orbiter Laser Altimeter topography of Valles Marineris and circum-Chryse chaos terrains and channels, at 0.25° resolution. (b) The same region with troughs, chaos, and channels removed. This topography is used for the second model variation discussed in section 2.3.

chaotic terrains, implying that some events occurred after the topography was significantly altered [*Harrison and Grimm*, 2008]. Nonetheless, it is important to consider the alternative end-member that disruption occurred prior to chaos and channel formation. Noting that the Valles Marineris troughs also contain chaotic terrains and give rise to outflow channels [*Chapman and Tanaka*, 2002], we consider an alternative model with an estimate of topography prior to both Valles Marineris and circum-Chryse chaos and outflow channel formation. The topography modification is performed on 0.25° gridded Mars Orbiter Laser Altimeter data (Figure 2) then coarsened to the model resolution of 2°.

2.3.3. Surface Breakout Pressure

[11] Nominally, we assume that heads must reach the local lithostatic value in order to disrupt the cryosphere. However, it is possible that extensive preexisting fracturing allowed groundwater to reach the surface at lower pressures. Indeed, the minimum head required for surface discharge is just the surface elevation. We adopt this as an alternative threshold breakout pressure (henceforth, we call the nominal and alternative values the "lithostatic breakout pressure" and "surface breakout pressure," respectively).

2.3.4. Permeability Length Scale

[12] We consider two variations to our stochastic permeability approach. In the first, we increase the length scale. The nominal choice of $R = 15°$ was driven by the average size of Martian photogeologic units. We also consider a value of 75°: this introduces more model-to-model variation in the net permeability between recharge and breakout locations, which are typically separated by much more than 15°. An example permeability distribution with this length scale is given in Figure 3.

2.3.5. Permeability Contrast

[13] We increase the standard deviation of $\log(k_{surf})$ from 0.5 to 1.0. However, we do not wish to change the maximum value because at −10 it corresponds to only 1 order of magnitude lower than the highest terrestrial values [*Domenico and Schwartz*, 1998]. Nor do we wish to change the mean value (−12.65), which would communicate changes to the overall time scale of breakout events in the model. We thus choose a formula that increases the contrast of the surface permeability values without changing the extrema, and with only small changes to the mean (no more than a few %). Our formula shifts each value toward the nearest of the two extrema by an amount that depends on its proximity to both the mean and that extremum. Specifically, each $\log(k_{surf})$ value in the random field (denoted k'_{old}) is replaced by the following new value:

$$k'_{new} = k'_{ext} + \left(k'_{old} - k'_{ext}\right)\left(\frac{k'_{old} - k'_{ext}}{k'_{old} - \langle k'_{old}\rangle}\right)^{n}$$

where $\langle k'_{old}\rangle$ is the mean of all $\log(k_{surf})$ values in the field, and n is a factor with a value of unity or higher depending on the degree of contrast desired (we use a value of 1.7). k'_{ext} is the nearest of the two $\log(k_{surf})$ extrema to k'_{old}. An example of the resulting permeability field is given in Figure 3. We perform this operation on the same 100 realizations used in the nominal model suite.

[14] Finally, because no two model variations in the above list are mutually exclusive, each of the 32 possible unique combinations must be considered. Because each combination involves a suite of 100 models (corresponding to 100 independent permeability fields), we run a total of 3200 models.

3. Results

[15] We first present results from the initial three model variations introduced in the previous section (i.e., only nominal permeability statistics are considered). From these variations, 8 unique combinations arise, each with 100 models

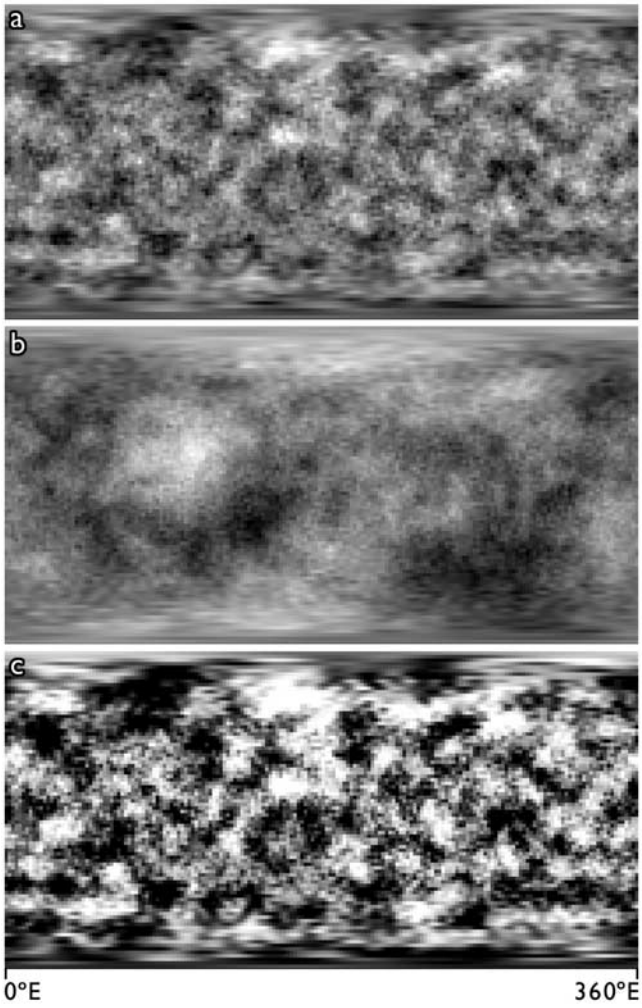

Figure 3. Example global maps of heterogeneous surface permeability, k_{surf}, plotted as $\log(k_{surf})$ over the range -14.1 to -10.9. In all cases, the mean value of $\log(k_{surf})$ is -12.7. (a) Nominal heterogeneous model ($R = 15°$, $\sigma = 0.5$). (b) Long length scale model ($R = 75°$, $\sigma = 0.5$). (c) High contrast model ($R = 15°$, $\sigma = 1.0$).

covering the same set of independent permeability realizations. For each combination, we bring the breakout locations from all 100 realizations together onto a single map (Figure 4). Circles indicate breakout sites, with circle diameter proportional to the number of models from the suite of 100 that produce a breakout at the finite difference cell corresponding to the circle center. Thus, the single large circle over Hellas in Figure 4a indicates that most models in the suite (97) produce a breakout at the same finite difference cell. Conversely, the group of small circles in Amazonis Planitia indicate that breakouts in this basin vary in location from one model to the next. We omit from Figure 4 any breakouts that are initiated later than 1 Ga: we regard this as a suitable upper limit to the period of outflow channel initiation that lasted from approximately the end of the Noachian to the early Amazonian. However, absolute initiation times depend somewhat on model permeability and the choice of initial head, both of which carry considerable uncertainty. The temporal ordering of different breakout locations is, on the other hand, comparatively robust.

[16] Results from model suites with the last two variations in the previous section (permeability contrast and length scale) show a somewhat greater number and spatial diversity of breakouts, but the general distribution seen in Figure 4 is conserved. (More generally we find that all heterogeneous permeability distributions essentially add varying degrees of spatial noise to the breakout locations observed in "control" models with homogeneous permeability.) Instead of providing breakout maps for model suites with the two permeability variations, we provide a quantitative overview of the entire modeling effort in Table 2. Specifically, we tabulate (for each of the 32 combinations arising from our five model variations) the total number of individual models (out of a possible 100) that produce breakouts in specific regions of Mars defined in Figure 5. We check the uncertainties in these results by considering the binomial distribution with 100 trials. The probability of a breakout is not fixed, but depends on geographic location: A value of 0.5 yields a maximum standard deviation of 5 breakouts, sufficiently small to justify the broad interpretations of the results presented below, and to justify our choice of 100 models in each suite.

[17] Finally, we note that model breakouts sometimes occur in impact craters. While craters might influence the precise location of breakout in a region of high pore pressures, they do not control the overall breakout pattern, and we did not remove any craters from the model topography. Nonetheless, we did investigate two craters (Lomonosov and Pettit) which produced a high number of model breakouts. Lomonosov (in Acidalia Planitia) produced the large circle at the top right corner of each of the lower four frames in Figure 4, while Pettit (in Amazonis Planitia) produced the medium to large circle near the center of each Tharsis recharge frame of Figure 4. Loose age constraints on these craters (Hesperian to Amazonian) [*Tanaka et al.*, 2005] raise the possibility that they were absent over the modeled period. We thus removed them from the topography in a copy of the nominal suite and the surface breakout pressure suite. In both cases, a few shifts in breakout location near the removed craters were observed but there was negligible change to the overall pattern or number of breakouts.

4. Discussion

[18] We begin discussion of our results by considering the first-order agreement between modeled and observed breakout locations. Because most of the Martian surface does not have chaotic terrains, the absence of breakouts in these regions (true negatives) is of limited significance. Regions without chaotic terrains but with high numbers of model breakouts (false positives) have important implications for groundwater flow, and are discussed in detail below. Importantly, no large chaotic terrains have high numbers of model breakouts (true positives). Instead, all chaotic terrains fall in the final category (false negatives), with implications also discussed below.

4.1. Absence of Chaotic Terrains at Preferred Model Breakout Locations

[19] The most likely model breakout site is Hellas Planitia (Table 2), which has the lowest topographic point on the

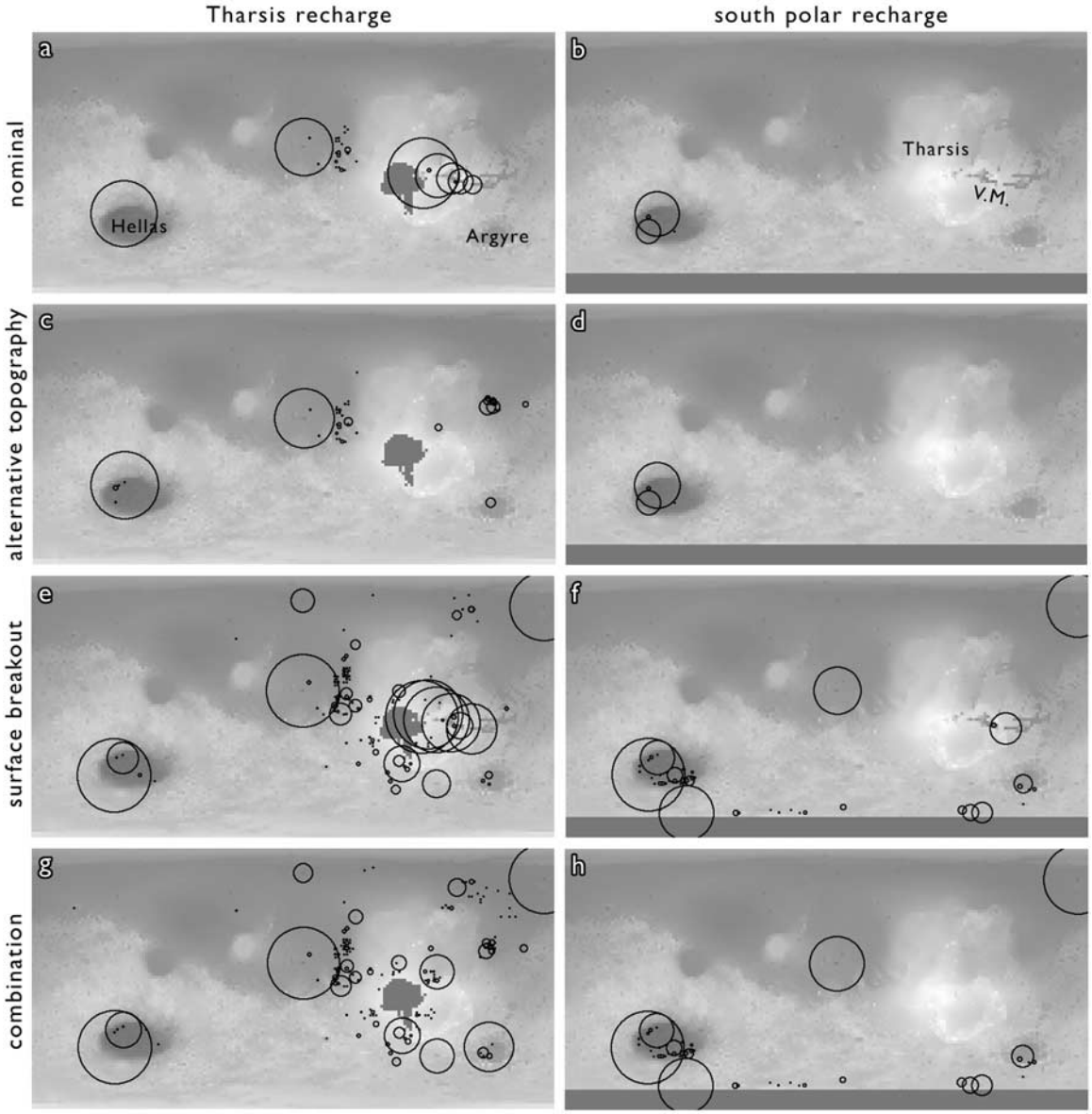

Figure 4. Compilation of breakout locations for nominal stochastic permeability models. Each frame superimposes breakouts from 100 independent simulations. Black circles are centered on breakouts, with circle diameter proportional to the number of models that experienced a breakout at the circle center (the largest circle, which appears over Hellas in frames e through h, corresponds to breakout in all 100 models). As indicated by uniformly gray areas, left frames have Tharsis recharge and right frames have south polar recharge. (a and b) Nominal models, (c and d) models with smoothed topography at Valles Marineris and circum-Chryse chaos and channels, (e and f) models with surface breakout pressure, and (g and h) combination of the two latter variations. Breakout locations adjacent to the recharge zone are omitted from all frames to reduce clutter. In addition, breakouts initiated after 1 Ga are omitted.

Martian surface (−8.2 km). Breakouts occur predominantly in the deepest part of the basin near its western rim, and are therefore significantly removed both laterally and vertically from the northeastern rim outflow channels.

[20] Hellas has been a sink for sedimentary and volcanic deposits since its formation in the Noachian [*Tanaka and Leonard*, 1995] and evidence of groundwater discharge contemporaneous with circum-Chryse chaotic terrain formation may be obscured or highly modified. Chaotic features are observed in Hellas, but they are widely thought to have resulted from the collapse of an ice-rich deposit due to volume loss associated with sublimation [*Sharp*, 1973; *Carr*, 1996; *Moore and Wilhelms*, 2001]. *Moore and Wilhelms* [2001], in postulating a Hellas paleolake, suggest groundwater seepage as a potential water source, but such seepage did not require wholesale cryosphere disruption. Given the great depth of Hellas, ponded water may have been deep enough to provide the crust with significant thermal insulation, allowing groundwater to discharge into the lake without the need for cryosphere disruption. Such a lake would have to

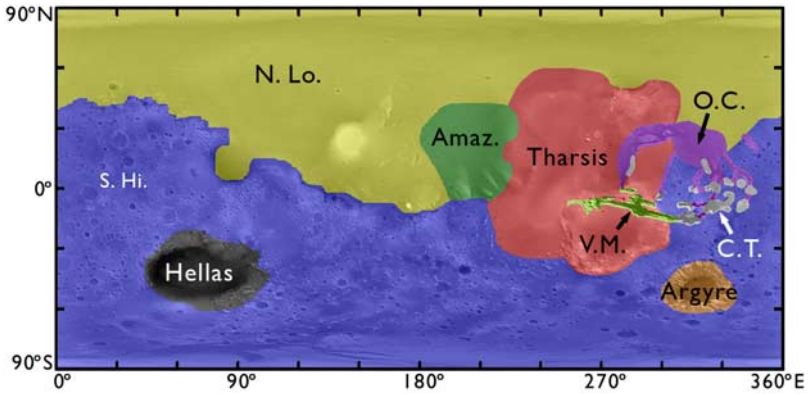

Figure 5. Map regions used to delineate breakout numbers in Table 2. Regions indicated by abbreviated labels are as follows: Amaz., Amazonis Planitia; C. T., chaotic terrains (circum-Chryse only); N. Lo., northern lowlands; O. C., outflow channels (circum-Chryse only); S. Hi., southern highlands; V. M., Valles Marineris.

form no later than the Noachian or early Hesperian, when precipitation was still occurring (episodically) and groundwater was not cut off from the surface by a cryosphere. If it formed too late in the Hesperian, the cryosphere would preclude groundwater input (the very reason for invoking a lake in the first place), but precipitation would have ceased also (as suggested by valley network ages) [*Fassett and Head*, 2008]. A late Noachian to early Hesperian formation time would require the lake to persist for up to 100 Ma, the minimum time required to achieve Hellas breakout in our models. It is not clear that a lake could last this long under atmospheric conditions similar to those of today. More detailed models with thermal and surface flow processes would be required to determine the importance of Hellas ponding to groundwater flow.

[21] Other regions without chaotic terrains but significant numbers of model breakouts include Amazonis and Chryse/Acidalia Planitiae. Amazonis borders the western flank of Tharsis, and its low elevation makes it a preferred breakout site in Tharsis recharge models. There are tentative indications of past groundwater or ground ice presence in Amazonis, including the Olympus Mons aureoles [*McGovern et al.*, 2004] and the northwestern slope valleys (putative outflow channels) [*Dohm et al.*, 2001]. However, the aureoles do not indicate groundwater-related cryosphere disruption, while support for outflow channel processes at the northwestern slope valleys is not definitive [*Dohm et al.*, 2001], and no chaotic terrain sources are observed (it is possible they were overlain by Arsia Mons lava flows).

[22] A few model breakouts occur near outflow channel outlets in Chryse Planitia and further north in Acidalia

Table 2. Number of Models Yielding Breakouts in Specific Regions of Mars[a]

	Nominal Topography								Modified Topography							
	Lithostatic Breakout Pressure				Surface Breakout Pressure				Lithostatic Breakout Pressure				Surface Breakout Pressure			
	R = 15°		R = 75°		R = 15°		R = 75°		R = 15°		R = 75°		R = 15°		R = 75°	
Map Region[b]	σ = 0.5	σ = 1.0	σ = 0.5	σ = 1.0	σ = 0.5	σ = 1.0	σ = 0.5	σ = 1.0	σ = 0.5	σ = 1.0	σ = 0.5	σ = 1.0	σ = 0.5	σ = 1.0	σ = 0.5	σ = 1.0
Tharsis Recharge																
S. Hi.	0	11	0	7	89	84	79	71	7	27	14	21	94	89	84	76
Hellas	91	62	83	55	100	100	100	100	100	93	95	67	100	100	100	100
Argyre	0	6	3	6	16	26	17	29	13	29	29	26	88	65	60	50
V. M.	100	100	100	97	100	100	100	100	0	0	0	0	100	100	100	100
O. C.	0	1	1	10	1	8	10	15	68	41	34	33	64	40	49	34
Tharsis	0	1	0	1	100	100	100	100	9	24	14	25	100	100	100	100
N. Lo.	79	60	65	41	100	98	98	82	81	66	64	43	100	99	100	89
Amaz.	42	62	48	52	93	79	78	66	48	68	51	55	93	81	80	67
C. T.	0	4	10	7	5	7	16	15	0	0	0	0	0	0	0	0
South Polar Recharge																
S. Hi.	0	0	0	0	100	100	100	100	0	0	1	4	100	100	100	100
Hellas	95	82	78	71	100	100	100	98	97	82	79	73	100	100	100	98
Argyre	0	0	0	0	36	40	37	43	0	0	0	0	41	45	46	50
V. M.	0	2	4	21	49	33	42	34	0	0	0	0	0	0	0	0
O. C.	0	0	0	0	0	0	0	0	0	0	0	0	0	0	0	0
Tharsis	0	0	0	0	0	0	0	0	0	0	0	0	0	0	0	0
N. Lo.	0	0	3	15	95	60	70	59	0	1	5	20	96	65	77	65
Amaz.	0	0	0	0	0	0	0	3	0	0	0	0	0	0	0	4
C. T.	0	0	0	0	0	3	0	7	0	0	0	0	0	0	0	0

[a]Number of models is out of a possible 100. Values are shown for all 32 combinations arising from the 5 model variations discussed in the text.
[b]See Figure 5 for a definition of each region and its shorthand label shown here.

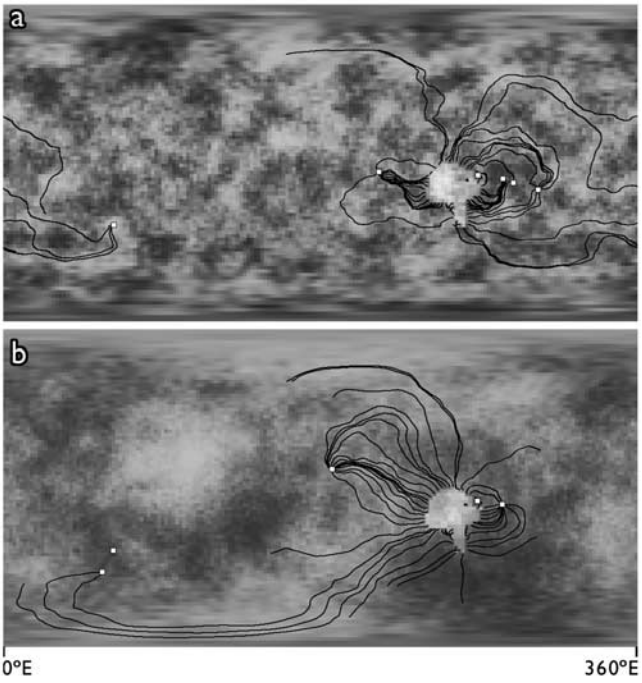

Figure 6. Pathlines in Tharsis recharge models taken from model suites with high permeability contrast and a permeability length scale of (a) 15° and (b) 75°. Surface permeabilities plotted as $\log(k_{surf})$ provide the background images. Lines are generated using the steady state solution for each model. They are initiated from model cells adjacent to the Tharsis recharge zone, and some terminate at breakout locations (white squares). Lines tend to follow regions of higher permeability. Breakout locations are broadly similar in Figures 6a and 6b, showing that topography dominates over permeability distribution.

Planitia. These regions also have low elevations relative to the Tharsis recharge zone. A geologic unit distinguished by knobs and mesas, interpreted by *Tanaka et al.* [2005] to have formed in the late Noachian to early Hesperian owing to collapse associated with basal seepage of volatiles, has an outcrop in Acidalia, suggesting a possible relationship to cryosphere disruption. However, more extensive outcrops of this unit are observed in other regions of Mars (mostly along the dichotomy boundary) where few model breakouts occur. It is therefore difficult to attribute this unit a significant association with modeled cryosphere disruption.

[23] Finally, a significant number of model breakouts are observed close to the recharge zone (in both Tharsis and south polar recharge models) for surface breakout pressure conditions. Since recharge is introduced at surface elevations, it is expected that nearby topographic lows will experience discharge under surface breakout conditions. However, the close proximity of these locations to recharge means that they are not relevant to the issue of global-scale flow. The lack of associated chaotic terrains most likely implies that pore pressures higher than the surface breakout condition were required for cryosphere disruption here.

[24] The principal conclusion that follows from the above results is that a general approach to global-scale groundwater flow driven by recharge at either Tharsis or the south polar region requires chaotic terrain formation where such terrains are not observed. This mismatch suggests at least one of two possibilities:

[25] 1. The Martian aquifer is not global. Our stochastic approach generally produces models with global-scale aquifers: High permeability zones are usually well connected, allowing the flow between any two points in the aquifer to be connected by a relatively high permeability pathway, albeit a tortuous one (Figure 6). We tested this phenomenon by running additional suites with very high permeability contrast ($\sigma = 4.0$) and with minimum surface permeabilities of about 10^{-20} m^2 (essentially impermeable). This approach ensures that moderately low permeability regions that may have accommodated the flow in the nominal permeability case are no longer accessible, thereby confining the flow to high permeability zones. The results did not deviate significantly from those contributing to Table 2, indicating that high permeability zones are indeed well connected. If such global hydrologic connectivity, expressed in the variety of forms from section 2.3, cannot produce the observed cryosphere disruption patterns, a likely conclusion is that the Martian aquifer is compartmented on a local to regional scale.

[26] Our models may fail to capture spatially limited flows for at least three reasons: (1) geologic formations that present barriers to groundwater flow (aquicludes) may be too small to be resolved by our model (i.e., narrower than 120 km); (2) aquicludes may be of a significantly different geometric shape to the generally amorphous low permeability zones produced by our stochastic approach (e.g., low permeability dike intrusions); and (3) aquicludes likely correspond to key Martian features (such as Tharsis) and are thus not randomly placed.

[27] 2. Martian groundwater was heterogeneously distributed. The inadequacy of global-scale groundwater flow implied by our model results may have arisen from an initially uneven distribution of groundwater, rather than from low permeabilities. Our models assume a steady supply of recharge able to raise heads globally given enough time. If, however, the initial distribution of water in the aquifer was heterogeneous, and if recharge was limited (in time or volume), then significant pore pressure increases would be limited to locations close to the recharge zone, leading to regional breakouts only. In this case, recharge over Tharsis could explain formation of the circum-Chryse outflow channels (as described below), but a separate source of recharge, or perhaps an entirely different mechanism, would be required to explain formation of the northeastern Hellas outflow channels.

[28] Conceivably, the location of aquifer recharge in our models could be iteratively modified until breakouts are predicted at the circum-Chryse and Hellas outflow channel source regions only, while allowing global-scale flow and avoiding both of the above scenarios. However, such modifications would likely result in recharge zones at high elevations close to the outflow channel heads, making global-scale flow implausible once again. Moreover, no suitable alternative recharge zone for the circum-Chryse outflows would likely be found, since Tharsis is the only nearby high-elevation region.

4.2. Absence of Model Breakouts at Chaotic Terrains

[29] The largest Martian chaotic terrains appear in the circum-Chryse region and along the northeastern rim of the

Hellas basin. Perhaps the most striking result of our modeling efforts is that breakouts are not generally predicted for either region (Figure 4 and Table 2). Only 16 of 100 models produce breakouts in the circum-Chryse chaotic terrain region of Figure 5 (Table 2). These occur for surface breakout pressure models with long path length permeability fields. Chaotic terrain breakouts occur almost exclusively in Hydraotes Chaos and to a lesser degree in Capri Chaos. The low elevation of these two terrains (Hydraotes has the lowest chaotic terrain elevation in the circum-Chryse region) makes them susceptible to high pore pressures. They also appear to have served as sinks for surface water, as suggested by terraces possibly formed at the shorelines of paleolake environments [*Ori and Mosangini*, 1998; *Harrison and Chapman*, 2008].

[30] No model breakouts occur in chaotic terrain regions if the terrains themselves have been removed from the topography. An assumption made in the topography removal process was that depressions containing chaotic terrain were wholly formed by chaos-related collapse. In many cases, however, depressions may have existed prior to chaotic terrain development. Shalbatana and Aram Chaotes likely formed in preexisting impact craters, while chaotic terrains in Valles Marineris troughs (Juventae, Ganges, Capri, etc.) may have formed after these troughs were opened by independent tectonic processes. The lack of chaotic terrain breakouts in alternative topography models is therefore not entirely unexpected. Nonetheless, it is clear that the regional elevation of the modeled circum-Chryse chaotic terrain environment is not generally conducive to breakout, even when the surface breakout pressure is used.

[31] Breakouts occur in Echus Chasma in a small number of models belonging to those suites that include both the alternative topography and the surface breakout pressure variations. Although Echus Chasma does not appear to contain chaotic terrain, its likely inundation by postoutflow deposits (interpreted by *Witbeck et al.* [1991] to be locally derived alluvial or aeolian material of Amazonian age) might have obscured the original channel source morphology [see *Harrison and Grimm*, 2008, Figure 6]. The lack of Echus breakouts in nominal topography models is due to the presence of the central Valles Marineris trough, where breakouts depress regional pore pressures, thereby preventing breakouts in neighboring canyons such as Echus, Hebes, and Juventae.

[32] As discussed above, many models produce breakouts in the Hellas basin (Table 2), but they occur predominantly in the deepest part of the basin near its western rim, and are therefore well separated from the northeastern rim outflow channels.

4.2.1. Valles Marineris

[33] The above results suggest an important role for the Valles Marineris canyons because aquifer drawdown due to breakouts in the canyons preclude breakouts that might occur elsewhere in the region, including the circum-Chryse chaotic terrains (in models with nominal topography). The floor of the central Valles Marineris trough system reaches elevations as low as 10 km below the nearby Tharsis recharge zone, making it a prime candidate for high pore pressures. Indeed, all Tharsis recharge models with nominal topography produce breakouts in the Valles Marineris, regardless of breakout pressure (Figure 4 and Table 2). Because the Valles Marineris canyons are close to Tharsis, breakouts are likely to have occurred there even if the Martian aquifer was locally or regionally limited as suggested above. Indeed, if large fractures were capable of funneling recharged groundwater downslope toward the Valles Marineris, or if precipitation could collect and melt directly in the canyons themselves, then a source of water for the outflow channels could be produced with very little influence from diffusive aquifer flow, rendering questions of canonical pore space permeability largely irrelevant. The presence of a spatially extensive, unaltered olivine-rich bedrock layer exposed by channel incision in the eastern Valles Marineris [*Christensen et al.*, 2003; *Edwards et al.*, 2008] appears to support the hypothesis that groundwater flow was not laterally pervasive but was focused at a few key locations such as fracture systems. (More generally, the heterogeneity of olivine-rich bedrock on Mars [*Hamilton and Christensen*, 2005] may support the second hypothesis of section 4.1, namely that the groundwater distribution on Mars was itself heterogeneous.)

[34] Fracture-sourced outflow channels are found at several other locations on Mars. On the high-elevation plateaus bordering the Valles Marineris canyons, small outflow channels with apparent fracture sources are observed [*Coleman et al.*, 2007]. Farther from the Valles Marineris, examples include Mangala Vallis [*Tanaka and Chapman*, 1990], Athabasca Vallis [*Burr et al.*, 2002], and channels emanating from various fossae in northern Tharsis [*Mouginis-Mark*, 1990]. It is interesting to note that Mangala Vallis and a set of chaotic terrains in Terra Sirenum [*Landheim*, 1995; *Head and Pratt*, 2001a] are both associated with fracture systems emanating from Tharsis (Memnonia and Sirenum Fossae, respectively). It seems likely then that the Valles Marineris fracture system, with its proximity to recharge over the Tharsis rise, and its large size, played a critical role in providing water for outflow channel formation. An important implication is that groundwater discharge at chaotic terrains may not be as significant as traditionally thought. If chaotic terrains can generally be shown to have only a weak association with groundwater discharge, then the low number of chaotic terrain breakouts in our models is no longer problematic (as discussed below). We emphasize, however, that the high breakout probabilities for regions such as Amazonis and Hellas (Table 2), where no evidence of breakouts is observed, still lead us to the conclusion that groundwater flow is (at most) local or regional in extent.

[35] Finally, while Valles Marineris tectonic structures may provide a means of delivering nearby Tharsis aquifer recharge to the circum-Chryse outflow channels, no obvious groundwater pathway to these channels exists for recharge at the south polar region. Indeed, our conclusion of regionally isolated groundwater flow makes a subsurface link between south polar recharge and the circum-Chryse outflow channels [*Clifford*, 1993] appear unlikely. Rather, meltwater at the south polar ice sheet likely flowed overland, possibly reaching the circum-Chryse region via Argyre Planitia [*Head and Pratt*, 2001b; *Grant and Parker*, 2002]. Furthermore, our conclusions support the parochial view of Noachian groundwater dynamics [*Grimm and Harrison*, 2003] in contrast to the large-scale flow required for a Noachian northern ocean [*Clifford and Parker*, 2001].

4.2.2. Hellas

[36] As suggested above, Tharsis and south polar recharge models are unable to produce breakouts where eastern Hellas

chaotic terrains are observed, and a nearby groundwater source is required instead. Chaotic terrain is found predominantly in only one Hellas outflow channel (Dao Vallis) and, while collapse appears to be an important contributor to its formation, the role of groundwater seems less certain, and is likely limited to a small initial flood and to later groundwater seepage [*Crown et al.*, 2005]. Nonetheless, if this terrain is indeed the result of groundwater-induced cryosphere disruption, then sufficient groundwater might have been delivered from the nearest high-elevation regions, namely, Hadriaca and Tyrrhena Paterae (both volcanic constructs) without the aid of global-scale flow. The head regions of two of the four northeastern Hellas valleys (Dao and Niger Valles) lie on the southern flanks of Hadriaca and close to the southwestern flanks of Tyrrhena. The remaining two valleys (Harmakhis and Reull Valles) appear to be joined [*Crown et al.*, 2005], and the resulting single head region cannot be traced to collapse or chaotic terrain features. The volume of material displaced from the Dao Vallis head region is on the order of 10^4 km^3 [*Musiol et al.*, 2008]. Adding a similar volume for the collapsed region of the Niger Vallis head, and making the generous assumption that all of this material was removed by fluvial processes, a sediment/water ratio of 0.67 [*Komar*, 1980] yields a water volume of 3×10^4 km^3. This volume could have been drawn from ice (melted by volcanic heat) in a 3 km deep cryosphere with a mean porosity of 0.017 (equation (A5)) and a lateral area of 6×10^5 km^2. Cryosphere melting at Hadriaca and Tyrrhena could have occurred over an area of 2×10^6 km^2, about three times the required value. If the sediment/water ratio was closer to terrestrial values (much lower than 0.67) [*Komar*, 1980] then provision of meltwater would become problematic. However, if collapse at Dao and Niger Valles is indeed taken as largely nonfluvial [*Crown et al.*, 2005], then the required volume of groundwater is greatly reduced. In summary then, it appears that Dao and Niger Valles could feasibly have relied on the regional aquifer only and that, unlike the circum-Chryse channels [*Harrison and Grimm*, 2004], they could have formed without aquifer recharge.

4.3. Role of Groundwater in Chaotic Terrains

[37] The support for aquifer compartmentalization presented above would be lost if chaotic terrains could be shown to have formed through processes other than groundwater-related cryosphere disruption. This may indeed be the case for the Hellas outflow channels and, plausibly, the circum-Chryse chaotic terrains. As discussed in the previous section, groundwater discharge may have contributed to small floods at the early stages of channel formation at Dao Vallis, and later to seepage processes not requiring cryosphere disruption [*Crown et al.*, 2005]. No obvious signs of catastrophic flooding, such as streamlines forms, inner channels, or scour features, are observed along Dao Vallis, although the possibility exists that such features have been erased by subsequent mass wasting processes [*Crown et al.*, 2005]. In the circum-Chryse region, the presence of inlet as well as outlet channels at most chaotic terrains may suggest that they formed in response to flow along existing drainage channels (or subsurface conduits) rather than by groundwater discharge [*Harrison*, 2009]. However, stronger support for this preliminary observation is required, and our work on this matter is ongoing.

5. Conclusions

[38] We ran a suite of Martian groundwater simulations geared toward testing the hypothesis that pore pressures in a globally connected aquifer could have produced cryosphere disruption where large chaotic terrains are observed. Our models include a variety of alternative initial conditions pertaining to the source of aquifer recharge required to elevate pore pressures, the threshold pore pressure required for disruption, and the topography of associated morphological features. Together with these variations, a range of stochastic heterogeneous permeability distributions provides a comprehensive and diverse set of models. Nonetheless, cryosphere disruption is not widely predicted for the circum-Chryse and eastern Hellas chaotic terrains, the traditionally accepted sources of groundwater discharge for outflow channel flooding. Even in the model suite with the most favorable initial conditions, only 16% of models produce cryosphere disruption at the circum-Chryse chaotic terrains. Furthermore, many models produce cryosphere disruption in Amazonis and western Hellas Planitae where no evidence of disruption is observed. We conclude that global-scale groundwater flow, even when limited to tortuous flow paths connecting regional high permeability zones, cannot produce a cryosphere disruption pattern commensurate with observations. It is thus likely that Martian groundwater flow was locally or regionally isolated.

[39] A further conclusion is that cryosphere disruption in the Valles Marineris canyon system (driven by aquifer recharge over Tharsis) is highly probable, even if groundwater flow is assumed to be regional. The position of the canyon system upstream of chaotic terrains suggests that groundwater discharge through Valles Marineris faults may have been a significant, if not dominant, source of water for outflow channel flooding. This mechanism already constitutes the standard formation model of outflow channels elsewhere on Mars, including Athabasca and Mangala Valles. Our results therefore suggest that the role of chaotic terrains in circum-Chryse outflow channel formation be carefully revisited and, if necessary, modified.

Appendix A: Model Details

[40] MODFLOW simulates changes in hydraulic head, which is measured relative to some arbitrary elevation (we use the Martian datum). Gradients in hydraulic head drive the flow of groundwater in a porous medium according to Darcy's law:

$$\vec{q} = -\frac{k\rho g}{\mu}\vec{\nabla}h \tag{A1}$$

where $\vec{q}$ is the volumetric flow rate per unit area, k is aquifer permeability (assumed isotropic here), ρ is fluid density, g is gravitational acceleration, μ is fluid viscosity, $\vec{\nabla}$ is the gradient operator, and h is hydraulic head. Together with conservation of mass, Darcy's law gives rise to the governing equation for groundwater flow [*Domenico and Schwartz*, 1998]:

$$s_s\frac{\partial h}{\partial t} = \frac{\rho g}{\mu}\vec{\nabla}\cdot\left(k\,\vec{\nabla}h\right) \tag{A2}$$

Specific storage s_s applies nominally to confined conditions and depends on the compressibilities of the aquifer and the pore fluid:

$$s_s = \rho g(\alpha + n\beta) \tag{A3}$$

[41] Here, α is the uniaxial compressibility of the porous medium, β is the compressibility of water, and n is the porosity of the medium. Parameter values used in equations (A2) and (A3) appear in Table 1. For unconfined conditions (occurring when an unsaturated zone exists below the cryosphere), MODFLOW uses a combination of specific storage and porosity that depends on the elevation of the water table relative to the finite difference cell being considered [*Harbaugh et al.*, 2000].

[42] Two features appear implicitly in equation (A2). The first is that permeability, while isotropic, is heterogeneous, allowing us to explore lateral variations in aquifer properties (Appendix B). The second is that temperature gradients are not considered important drivers of groundwater flow in the current context. However, the thermal state of the crust does constrain aquifer geometry: the upper boundary of the aquifer (defined by the bottom of the impermeable cryosphere) is determined by the melting isotherm, itself a function of surface temperature, crustal heat flux, and topography (Table 1). The heat flux in particular is quite poorly constrained and it is possible that significant regional variations produced correspondingly variable cryosphere thicknesses. In lieu of better constraints, however, we assume uniform heat flux.

[43] We model the depth dependence of permeability using the power law derived from terrestrial observations [*Manning and Ingebritsen*, 1999] and adapted to Mars [*Clifford and Parker*, 2001]:

$$\log k = -12.65 - 3.2 \log z \tag{A4}$$

where z is depth below the surface, in km. Because of the singularity at $z = 0$, we assume that the top 1 km of the crust has a constant nominal permeability given by the $z = 1$ value (2.2×10^{-13} m^2). Because the cryosphere ranges in thickness from about 3 to 5 km (see cryosphere thermal properties in Table 1), the aquifer lies below $z = 1$ km and is not influenced by this assumption (the single exception is the recharge zone, where there is no cryosphere). Laterally, permeability is allowed to vary stochastically about the equation (A4) value (Appendix B). We also use equation (A4) to determine the lower boundary of the aquifer. This boundary is often defined by the depth at which pore space closes owing to the transition in crustal properties from brittle to plastic. However, there is a wide range of possible values (10 to 20 km) [*Hanna and Phillips*, 2005] and we choose instead the depth (19 km) that would accommodate 95% of the horizontal groundwater flux expected in an infinitely deep aquifer with the permeability-depth dependence of equation (A4).

[44] Porosity is also assumed to decrease with depth and is derived directly from the permeability using the Kozeny-Carman relation [*Saar and Manga*, 1999], yielding

$$\log n = -1.65 - 0.8 \log z \tag{A5}$$

The $z = 1$ km permeability (2.2×10^{-13} m^2) gives rise to a porosity of 0.02. However, our models operate predominantly under confined conditions, limiting the influence of porosity to its relatively weak role in the specific storage expression of equation (A3) (the two compressibilities are of similar magnitude; Table 1).

[45] One of our central goals here is to explore a suitable portion of the relevant parameter space, requiring us to run a large number of models. The associated computational constraints restrict us to single-layer models and therefore to equation (A4) permeabilities averaged over depth. This simplification is likely to influence the local flow at breakout and recharge locations only, since this is where a vertical flow component is expected. For lateral discretization we use a 2 degree (at most 120 km) resolution capable of capturing the expected regional and global horizontal head gradients.

[46] For completeness, we define lithostatic head, the nominal threshold hydraulic head required for cryosphere breakout:

$$h_{litho} = \frac{W}{\rho g} + z_0 \tag{A6}$$

where z_0 is lower boundary elevation of the cryosphere and W is the weight of the overlying cryosphere column of unit cross-sectional area, given by

$$W = \rho_{ice} g N + \rho_{rock} g (L - N) \tag{A7}$$

Here, N is the total pore volume of the cryosphere column obtained by integrating equation (A5) over the cryosphere thickness L, yielding units of length (L^3/L^2). ρ_{ice} and ρ_{rock} are water ice and rock densities, respectively (Table 1). Quantities in equations (A6) and (A7) are functions of latitude and longitude, with the exception of the three densities and g.

[47] To increase pore pressures for cryosphere disruption, a driving force is required, and must be included explicitly in any self-consistent model geared toward prediction of cryosphere disruption location. Candidates include aquifer recharge and downward cryosphere growth. The latter process does not seem readily able to produce the required pressures [*Hanna and Phillips*, 2005; *Wang et al.*, 2006], while recharge at any elevation above the superlithostatic head elevation of a nearby point on the topography has the potential to cause disruption at that point. Aquifer recharge is more widely supported [e.g., *Clifford and Parker*, 2001; *Russell and Head*, 2007] and, as suggested above, is likely required in order to deliver large groundwater volumes to the circum-Chryse outflow channels [*Harrison and Grimm*, 2004]. We thus adopt recharge as our principal source of pore pressure, applying a maximum rate of 2×10^{-10} m.s^{-1} [*Clifford and Parker*, 2001] alternatively to the high-elevation Tharsis rise and to the south polar region. (Recharge is not forced into the aquifer: if it cannot be accommodated, it is assumed to be lost as surface runoff.) For Tharsis recharge, we use the area of the south polar cap as a likely ice sheet size (approximately 2×10^6 km^2), which also makes comparison with south polar recharge models more balanced. We place the recharge area over the highest parts of Tharsis that remain after subduing

Amazonian volcanic edifices. Recharge elevation, rather than area, is likely to be the stronger influence on breakout location, since it places an upper bound on aquifer heads.

[48] Our models are initially unconfined, with a uniform water table low enough to avoid superlithostatic pore pressures at any point. Variations in this initial level are expected to have only a small influence on the timing and location of breakouts: timing is controlled by the lateral propagation of elevated pore pressures, and location is determined largely by the relationship between topography and recharge elevation. As depicted in Figure 1, recharge raises the local water table to the top of the aquifer and proceeds to spread high pore pressures radially outward. If continued increases in pore pressure result in superlithostatic values (and therefore a breakout) at a given location, the head boundary condition at the superlithostatic model cell is moved to the topographic surface, allowing discharge to occur through the upper cell surface, which in turn brings pore pressures down. If discharge ceases, the cryosphere is assumed to refreeze and head is free to increase once again. Although the discharge rate during a breakout event is recorded, the fate of the water once it reaches the surface is ignored. We therefore do not account for any changes in the breakout cell head brought about by ponding of surface water. Such changes are expected to occur very slowly because a given drawdown in the aquifer produces a much smaller increase in lake elevation, by a factor approximately equal to the porosity, and even less if the lateral extent of the ponded body is large. Lake bodies on Mars are not expected to remain fluid (and therefore coupled to the groundwater system) for more than a few thousand years [*Kreslavsky and Head*, 2002] which is short relative to regional changes in hydraulic head.

Appendix B: Heterogeneous Permeability Fields

[49] For a random scalar field defined on a 2-D domain, a variogram describes the statistical variance between two values of the scalar as a function of their spatial separation. Points closest together are usually most strongly correlated (lowest variance), and as separation increases the variance also increases until a constant value (the "sill") is reached. The sill is equivalent to the sample variance of the entire data set. The separation at which the sill is reached (the "range") gives the approximate correlation length scale of the scalar. On a sphere, separation is the geodesic distance between the two points. However, we use here the proportional quantity of angular separation because it is independent of the radius of the sphere. Furthermore, rather than calculating the variogram of a given map of scalar values, we require the reverse, namely to generate a map from a model (theoretical) variogram with a desired range and sill. Our method is described below.

[50] We choose the commonly used spherical variogram [*Chiles and Delfiner*, 1999] with a sill c and range R, and we define the covariance $K(\theta) = c - \gamma(\theta)$ where $\gamma(\theta)$ is the semivariogram (half the variogram). Our approach is to use this covariance to determine the coefficients of a Fourier-Legendre series representing the spherical (2-D) scalar field [*Obukhov*, 1947; *Hannan*, 1970]. Each term in the series will give us control over a particular spatial wavelength, and therefore over the resulting correlation length scale of the scalar field. Accordingly, we construct the following Fourier-Legendre expansion of $K(\theta)$

$$K(\theta) = \sum_{n=0}^{\infty} K_n P_n(\cos\theta) \tag{B1}$$

where $P_n(\cos\theta)$ is the nth Legendre polynomial. The coefficients K_n are as follows [*Kaplan*, 1992]:

$$K_n = \frac{2n+1}{2} \int_{-1}^{1} P_n(\cos\theta) K(\theta) d(\cos\theta) \tag{B2}$$

The K_n can be computed using our initial definition of $K(\theta)$.

[51] We denote as $f(\mathbf{r})$ the random scalar field we wish to simulate on the sphere, where $\mathbf{r}$ is the position of a point on the sphere. We write f as an expansion of spherical harmonics:

$$f(\mathbf{r}) = \sum_{n=0}^{\infty} \sum_{m=-n}^{n} f_{nm} Y_{nm}(\mathbf{r}) \tag{B3}$$

where f_{nm} are complex scalar coefficients and $Y_{nm}(\mathbf{r})$ are spherical harmonics of degree n and order m. The determination of the f_{nm} involves the K_n from the previous step. Specifically, the Legendre polynomials in equation (B2) can be rewritten in terms of spherical harmonics and then substituted for the spherical harmonics in equation (B3). The result is an expression for the covariances of the f_{nm}:

$$\langle |f_{nm}|^2 \rangle = \frac{4\pi K_n}{2n+1} \tag{B4}$$

This expression, which is independent of m, can be evaluated using the K_n of equation (B2). The random nature of the scalar field is implemented by choosing random values of f_{nm} for input into equation (B3). However, the variance of these values must be governed by the model variogram, and must therefore be constrained by equation (B4). We thus proceed by selecting the f_{nm} from a Gaussian distribution with zero mean and unity variance and multiplying by the square root of the variance in equation (B4). Once all the f_{nm} are selected, the scalar field is generated through equation (B3). The real and imaginary parts of $f(\mathbf{r})$ are independent and can both be used as realizations of the scalar field.

[52] **Acknowledgments.** This work was supported by NASA grants NNG05GL83G and NNG05GL22G. We thank Neil Coleman and Jules Goldspiel for insightful reviews.

References

Andrews-Hanna, J. C., and R. J. Phillips (2007), Hydrological modeling of outflow channels and chaos regions on Mars, *J. Geophys. Res.*, *112*, E08001, doi:10.1029/2006JE002881.

Baker, V. R. (1982), *The Channels of Mars*, Univ. of Tex. Press, Austin, Tex.

Burr, D. M., J. A. Grier, A. S. McEwen, and L. P. Keszthelyi (2002), Repeated aqueous flooding from the Cerberus Fossae: Evidence for very

recently extant, deep groundwater on Mars, *Icarus*, *159*, 53–73, doi:10.1006/icar.2002.6921.
Carr, M. H. (1979), Formation of Martian flood features by release of water from confined aquifers, *J. Geophys. Res.*, *84*, 2995–3007, doi:10.1029/JB084iB06p02995.
Carr, M. H. (1996), *Water on Mars*, Oxford Univ. Press, New York.
Carr, M. H. (2002), Elevations of water-worn features on Mars: Implications for circulation of groundwater, *J. Geophys. Res.*, *107*(E12), 5131, doi:10.1029/2002JE001845.
Chapman, M. G., and K. L. Tanaka (2002), Related magma-ice interactions: Possible origins of chasmata, chaos, and surface materials in Xanthe, Margaritifer, and Meridiani Terrae, Mars, *Icarus*, *155*, 324–339, doi:10.1006/icar.2001.6735.
Chiles, J. P., and P. Delfiner (1999), *Geostatistics: Modeling Spatial Uncertainty*, John Wiley, New York.
Christensen, P. R., et al. (2003), Morphology and composition of the surface of Mars: Mars Odyssey THEMIS results, *Science*, *300*, 2056–2061, doi:10.1126/science.1080885.
Clifford, S. M. (1993), A model for the hydrologic and climatic behavior of water on Mars, *J. Geophys. Res.*, *98*, 10,973–11,016, doi:10.1029/93JE00225.
Clifford, S. M., and T. J. Parker (2001), The evolution of the Martian hydrosphere: Implications for the fate of a primordial ocean and the current state of the northern plains, *Icarus*, *154*, 40–79, doi:10.1006/icar.2001.6671.
Coleman, N. M., C. L. Dinwiddie, and K. Casteel (2007), High outflow channels on Mars indicate Hesperian recharge at low latitudes and the presence of canyon lakes, *Icarus*, *189*, 344–361, doi:10.1016/j.icarus.2007.01.020.
Craddock, R. A., and A. D. Howard (2002), The case for rainfall on a warm, wet early Mars, *J. Geophys. Res.*, *107*(E11), 5111, doi:10.1029/2001JE001505.
Crown, D. A., L. F. Bleamaster, and S. C. Mest (2005), Styles and timing of volatile-driven activity in the eastern Hellas region of Mars, *J. Geophys. Res.*, *110*, E12S22, doi:10.1029/2005JE002496.
Dohm, J. M., et al. (2001), Latent outflow activity for western Tharsis, Mars: Significant flood record exposed, *J. Geophys. Res.*, *106*, 12,301–12,314, doi:10.1029/2000JE001352.
Domenico, P. A., and F. W. Schwartz (1998), *Physical and Chemical Hydrogeology*, John Wiley, New York.
Edwards, C. S., P. R. Christensen, and V. E. Hamilton (2008), Evidence for extensive olivine-rich basalt bedrock outcrops in Ganges and Eos chasmas, Mars, *J. Geophys. Res.*, *113*, E11003, doi:10.1029/2008JE003091.
Fassett, C. I., and J. W. Head (2008), The timing of Martian valley network activity: Constraints from buffered crater counting, *Icarus*, *195*, 61–89, doi:10.1016/j.icarus.2007.12.009.
Gendrin, A., et al. (2005), Sulfates in Martian layered terrains: The OMEGA/Mars Express view, *Science*, *307*, 1587–1591, doi:10.1126/science.1109087.
Grant, J. A., and T. J. Parker (2002), Drainage evolution in the Margaritifer Sinus region, Mars, *J. Geophys. Res.*, *107*(E9), 5066, doi:10.1029/2001JE001678.
Grimm, R. E., and K. P. Harrison (2003), A parochial view of groundwater flow on Mars, *Lunar Planet. Sci.*, *XXXIV*, Abstract 2053.
Grotzinger, J. P., et al. (2005), Stratigraphy and sedimentology of a dry to wet eolian depositional system, Meridiani Planum, Mars, *Earth Planet. Sci. Lett.*, *240*, 11–72, doi:10.1016/j.epsl.2005.09.039.
Haberle, R. M., J. R. Murphy, and J. Schaeffer (2003), Orbital change experiments with a Mars general circulation model, *Icarus*, *161*, 66–89, doi:10.1016/S0019-1035(02)00017-9.
Hamilton, V. E., and P. R. Christensen (2005), Evidence for extensive, olivine-rich bedrock on Mars, *Geology*, *33*, 433–436, doi:10.1130/G21258.1.
Hanna, J. C., and R. J. Phillips (2005), Hydrological modeling of the Martian crust with application to the pressurization of aquifers, *J. Geophys. Res.*, *110*, E01004, doi:10.1029/2004JE002330.
Hannan, E. J. (1970), *Multiple Time Series*, John Wiley, New York.
Harbaugh, A. W., E. R. Banta, M. C. Hill, and M. G. McDonald (2000), MODFLOW-2000, the U.S. Geological Survey modular ground-water model: User guide to modularization concepts and the ground-water flow process, *U.S. Geol. Surv. Open File Rep. 00–92*, 121 pp.
Harrison, K. P. (2009), An alternative view of Martian chaotic terrain formation, *Lunar Planet. Sci.*, *XXXX*, Abstract 1743.
Harrison, K. P., and M. G. Chapman (2008), Evidence for ponding and catastrophic floods in central Valles Marineris, Mars, *Icarus*, *198*, 351–364.
Harrison, K. P., and R. E. Grimm (2004), Tharsis recharge: A source of groundwater for Martian outflow channels, *Geophys. Res. Lett.*, *31*, L14703, doi:10.1029/2004GL020502.
Harrison, K. P., and R. E. Grimm (2008), Multiple flooding events in Martian outflow channels, *J. Geophys. Res.*, *113*, E02002, doi:10.1029/2007JE002951.
Head, J. W., and S. Pratt (2001a), Closed chaos basins on Mars: Evidence for regional groundwater drawdown and collapse, *Lunar Planet. Sci.*, *XXXII*, Abstract 1774.
Head, J. W., and S. Pratt (2001b), Extensive Hesperian-aged south polar ice sheet on Mars: Evidence for massive melting and retreat, and lateral flow and ponding of meltwater, *J. Geophys. Res.*, *106*, 12,275–12,300, doi:10.1029/2000JE001359.
Kaplan, W. (1992), Fourier-Legendre series, in *Advanced Calculus*, 4th ed., pp. 508–512, Addison-Wesley, Redwood City, Calif.
Komar, P. D. (1980), Modes of sediment transport in channelized water flows with ramifications to the erosion of the Martian outflow channels, *Icarus*, *42*, 317–329, doi:10.1016/0019-1035(80)90097-4.
Kreslavsky, M. A., and J. W. Head (2002), Fate of outflow channel effluents in the northern lowlands of Mars: The Vastitas Borealis Formation as a sublimation residue from frozen ponded bodies of water, *J. Geophys. Res.*, *107*(E12), 5121, doi:10.1029/2001JE001831.
Landheim, R. (1995), Exobiology sites for Mars exploration and geologic mapping of Gusev crater-Ma'adim Vallis, M.S. thesis, 167 pp., Ariz. State Univ., Tempe.
Luo, W., and A. D. Howard (2008), Computer simulation of the role of groundwater seepage in forming Martian valley networks, *J. Geophys. Res.*, *113*, E05002, doi:10.1029/2007JE002981.
MacKinnon, D. J., and K. L. Tanaka (1989), The impacted Martian crust: Structure, hydrology, and some geologic implications, *J. Geophys. Res.*, *94*, 17,359–17,370, doi:10.1029/JB094iB12p17359.
Manga, M. (2004), Martian floods at Cerberus Fossae can be produced by groundwater discharge, *Geophys. Res. Lett.*, *31*, L02702, doi:10.1029/2003GL018958.
Manning, C. E., and S. E. Ingebritsen (1999), Permeability of the continental crust: Implications of geothermal data and metamorphic systems, *Rev. Geophys.*, *37*, 127–150, doi:10.1029/1998RG900002.
McDonald, M. G., and A. W. Harbaugh (1988), A modular three-dimensional finite-difference ground-water flow model1988, *U.S. Geol. Surv. Tech. Water Resour. Invest., Book 6, Chap. A1*, 586 pp.
McGovern, P. J., S. C. Solomon, D. E. Smith, M. T. Zuber, M. Simons, M. A. Wieczorek, R. J. Phillips, G. A. Neumann, O. Aharonson, and J. W. Head (2002), Localized gravity/topography admittance and correlation spectra on Mars: Implications for regional and global evolution, *J. Geophys. Res.*, *107*(E12), 5136, doi:10.1029/2002JE001854.
McGovern, P. J., J. R. Smith, J. K. Morgan, and M. H. Bulmer (2004), Olympus Mons aureole deposits: New evidence for a flank failure origin, *J. Geophys. Res.*, *109*, E08008, doi:10.1029/2004JE002258.
Moore, J. M., and D. E. Wilhelms (2001), Hellas as a possible site of ancient ice-covered lakes on Mars, *Icarus*, *154*, 258–276, doi:10.1006/icar.2001.6736.
Mouginis-Mark, P. J. (1990), Recent water release in the Tharsis region of Mars, *Icarus*, *84*, 362–373, doi:10.1016/0019-1035(90)90044-A.
Musiol, S., S. van Gasselt, and G. Neukum (2008), Channel geometry and discharge estimates for Dao and Niger Valles, Mars, *Eur. Planet. Sci. Cong.*, *3*, Abstract EPSC2008-A-00438.
Obukhov, A. M. (1947), Statistically homogeneous fields on a sphere, *Usp. Mat. Nauk*, *2*, 196–198.
Ori, G. G., and C. Mosangini (1998), Complex depositional systems in Hydraotes Chaos, Mars: An example of sedimentary process interactions in the Martian hydrologic cycle, *J. Geophys. Res.*, *103*, 22,713–22,723, doi:10.1029/98JE01969.
Poulet, F., J.-P. Bibring, J. F. Mustard, A. Gendrin, N. Mangold, Y. Langevin, R. E. Arvidson, B. Gondet, C. Gomez, and the Omega Team (2005), Phyllosilicates on Mars and implications for early Martian climate, *Nature*, *438*, 623–627, doi:10.1038/nature04274.
Russell, P. S., and J. W. Head (2007), The Martian hydrologic system: Multiple recharge centers at large volcanic provinces and the contribution of snowmelt to outflow channel activity, *Planet. Space Sci.*, *55*, 315–332, doi:10.1016/j.pss.2006.03.010.
Saar, M. O., and M. Manga (1999), Permeability-porosity relationship in vesicular basalts, *Geophys. Res. Lett.*, *26*, 111–114, doi:10.1029/1998GL900256.
Sharp, R. P. (1973), Mars: Troughed terrain, *J. Geophys. Res.*, *78*, 4063–4072, doi:10.1029/JB078i020p04063.
Tanaka, K. L., and M. G. Chapman (1990), The relation of catastrophic flooding of Mangala Valles, Mars, to faulting of Memnonia Fossae and Tharsis volcanism, *J. Geophys. Res.*, *95*, 14,315–14,323, doi:10.1029/JB095iB09p14315.
Tanaka, K. L., and G. J. Leonard (1995), Geology and landscape of the Hellas region of Mars, *J. Geophys. Res.*, *100*, 5407–5432, doi:10.1029/94JE02804.

Tanaka, K. L., J. A. Skinner, and T. M. Hare (2005), Geologic map of the northern plains of Mars, scale 1:15M, *U.S. Geol. Surv. Sci. Invest. Map 2888*.

Tóth, J. (1963), A theoretical analysis of groundwater flow in small drainage basins, *J. Geophys. Res.*, *68*, 4795–4812, doi:10.1029/JZ068i008p02354.

Wang, C., M. Manga, and J. C. Hanna (2006), Can freezing cause floods on Mars?, *Geophys. Res. Lett.*, *33*, L20202, doi:10.1029/2006GL027471.

Witbeck, N. E., K. L. Tanaka, and D. H. Scott (1991), Geologic map of the Valles Marineris region, Mars, *U.S. Geol. Surv. Misc. Inv. Ser. Map I-2010*.

R. E. Grimm and K. P. Harrison, Southwest Research Institute, 1050 Walnut Street, Suite 300, Boulder, CO 80302, USA. (harrison@boulder.swri.edu)